doi:10.5937/jaes16-17249 Paper number: 16(2018)2, 522, 225 - 232

BURNED AREA RECOGNITION BY CHANGE DETECTION ANALYSIS USING IMAGES DERIVED FROM SENTINEL-2 SATELLITE: THE CASE STUDY OF SORRENTO PENINSULA,ITALY

Massimiliano Pepe* Cluadio Parente

University of Naples "Parthenope", Department of Sciences and Technologies, Italy

The purpose of this paper is to identify the burned areas that occurred in Italy during the summer of 2017 using change detection analysis techniques. This task is possible thanks to continuous, free and open availability of the multispectral images obtained by Sentinel-2 satellites. Indeed, comparing the satellite images of the same scene recorded at different times, it was possible to evaluate the landscape change. In this paper, the Direct Comparison change detection technique was applied to the analysis and identification of burned area using several Remote Sensing indexes. In particular, in order to achieve this aim, NBR (Normalized Burn Ratio) and NDVI (Normalized Difference Vegetation Index) were used. By case study in South Italy region (Sorrento peninsula), using images derived from Sentinel-2A imagery, it was possible to identify the burned areas in a specific period and evaluate the performance of the two indexes. In fact, after having constructed the confusion matrix for the two tested indexes, through the use of methods that indicate the quality of a thematic map (User's Accuracy, Producer's Accuracy, Overall Accuracy and Kappa coefficient), the percentage values for each remote sensing index analyzed were compared. The analysis of the different methods revealed, from one side the high quality of the results achievable by NBR index, on the other side, it was shown how, in some areas, the NDVI was inadequate for the recognition of burned areas.

Key words: NBR, NDVI, Burns, Sentinel-2, Change Detection, Thematic-map

INTRODUCTION

During the summer of the year 2017, the Italian territory was devastated by numerous and dramatic fires which destroyed extended forest areas [01]. In these burned areas also important valuable plant landscapes were involved, such as the mountains of the *Vesuvius* and the *Lattari* mountains, located in south of Italy. According to Italian law (Law 21 November 2000, no. 353) on the areas hit by fires, a building ban is imposed for a period of 15 years (except if the purpose of the project is of public utility). Also, considering the importance of this constraint, the identification of these areas plays an important role for land owners.

In order to identify the burned areas, in the Remote Sensing (RS) field, several approaches have been implemented [02, 03]. A widely used method is the so-called "*change detection analysis*" (*CDA*) which allows to show the land transformations by comparing images related to the same scene but recorded in different periods. In general, the *Change Detection* techniques can be divided in two macro areas [04]: *Direct Comparison* (or *Pre-Classification Comparison*) and *Post-Classification Comparison*. For the present study, the first technique, which provides the images comparison before their classification (Image differencing), is adopted. In particular, the first step used in this paper, was the calculation of vegetation index and, subsequently to perform the different maps referred to two specific times, i.e. carrying out the so-called *Vegetation Index Differencing* (*VDI*).

In the context of the identification of burned areas, a popular approach is based on the creation of the difference of Normalized Difference Vegetation Index (NDVI) calculated on satellite images in two steps: pre-fire and post-fire. The NDVI, as is well known in the literature [05,06,07,08], can be defined as the normalized ratio of the difference of the near-infrared and red bands, as shown in the equation 1:

$$NDVI = \frac{\rho_{NIR} - \rho_{Red}}{\rho_{NIR} + \rho_{Red}} \quad 1)$$

where ρ is reflectance, and the subscripts *NIR* and *Red* describe the respective spectral regions. The differenced *NDVI* index (*dNDVI*), that is the difference between $NDVI_{pre\text{-}fire}$ and $NDVI_{post\text{-}fire}$, has been successfully adopted in burned land discrimination [09, 10, 11].

Based on the potential of the mid-infrared region of the spectrum, in RS field the *NBR* (Normalized Burn Ratio) index has been developed (Formula 2), whose formula is similar to *NDVI* and can be defined as [12,13,14]:

$$NBR = \frac{\rho_{NIR} - \rho_{SWIR}}{\rho_{NIR} + \rho_{SWIR}} \quad 2)$$

where ρ is reflectance, and the subscripts *NIR* means near-infrared and *SWIR* means shortwave-infrared. In the same way used for *NDVI*, it is possible to build the differenced *NBR* index (*dNBR*) as the difference between $NBR_{pre\text{-}fire}$ and $NBR_{post\text{-}fire}$ [15,16].

* *University of Naples "Parthenope", Via Amm. F. Acton, 38 - 80133 Napoli, Italy, massimiliano.pepe@uniparthenope.it*

Observing the formulas (1) and (2), it is possible to note how the *NIR*, *Red* and *SWIR* are the most suitable bands to describe the burned vegetation. To test these indexes, the images from Sentinel-2, an Earth observation mission developed by *ESA* (European Space Agency) as part of the Copernicus Programme, were taken into consideration in this work.

MATERIALS AND METHODS

Study area

The study area concerns part of the "*Monti Lattari*" located in Campania region, southern Italy. Because of the high temperatures achieved during the summer, the drought and illegality phenomena, great areas belonging to the "*Regional Park of Monti Lattari*" were devoured by fires. Indeed, as shown in the Figure 1, the Copernicus Sentinel-2B satellite recorded on 12 July 2017 an image that shows the severity and extent of the vegetation burned in the study area.

In particular, the subset taken in consideration is located approximately between 14°17'28" and 14°45'47" East longitude and between 40°33'31" and 40°44'26" North latitude (reference system: WGS84). In the Figure 1 plane coordinates referred to UTM-WGS84, zone 33 N are shown in the band compositions: Visible (*Red-Green-Blue*); Color Infrared (*Red-Green-Near Infrared*); False color (*Red-Green-Short Wave Infrared*). In this area, the vegetation landscape varies according to the altitude: in the areas next to the sea there are the carob and the olive, in the intermediate area prevail the holm oak, the flowering ash, the oak and shrubs like the strawberry tree and the heather while in the greater altitude there are many chestnut and alder, but also hornbeam, ash and beech [17].

Satellite platform

In order to identify burned areas, images derived by Sentinel-2 satellite platform, were taken in consideration.

The Sentinel-2 is provided of multi-spectral instrument (MSI) able to acquire with 13 spectral channels in the visible/near infrared and short wave infrared spectral range. As concerning the spatial resolution, the MSI instruments acquires in different mode. In particular, four bands at 10 m geometric resolution: Blue (B2: 439–535 nm), Green (B3: 537-582 nm), Red (B4: 646-685 nm), Near Infrared (B4: 646-685 nm); six bands at 20 m geometric resolution: Vegetation Red Edge 1-VRE1 (B5: 694-714 nm), Vegetation Red Edge 2-VRE2 (B6: 731-749 nm), Vegetation Red Edge 3-VRE3 (B7: 768-796 nm), Narrow Near Infrared-NIR (B8: 767-908 nm), short wave infrared spectral range 1-SWIR1 (B11: 1539-1681 nm), shortwave infrared spectral range 2- SWIR2 (B12: 2072-2312 nm); three bands at 60 m geometric resolution: Coastal Aerosol-C/A(B1: 421-457 nm), Water vapour (B9: 931-958 nm) and short wave infrared spectral range Cirrus (B10: 1338-1414 nm) [18,19]. In the case of Sentinel-2 image, the formulation of *NDVI* and *NBR* indexes are (Formula 2-3):

$$NDVI = \frac{B8 - B4}{B8 + B4} \quad 3)$$

$$NBR = \frac{B8 - B12}{B8 + B12} \quad 4)$$

Datasets

The Sentinel-2A datasets used in this study are the standard Level-1C products, were produced by radiometric and geometric corrections, including ortho-rectification and spatial registration on a global reference system with sub-pixel accuracy. The Sentinel-2 datasets have been downloaded from ESA (European Space Agency) website (https://scihub.copernicus.eu/). The two best datasets suitable for the study, pre and post fire of the 12th July 2017, are:

S2A_MSIL1C_20170707T095031_N0205_R079_T33TVF_20170707T095257.SAFE
- RECORDED DATA: 7TH JULY 2017

S2B_MSIL1C_20170801T095029_N0205_R079_T33TVF_20170801T095712.SAFE
- RECORDED DATA: 1TH AUGUST 2017

In both datasets, the coordinate system is WGS84/UTM 33 and, from the radiometric point of view, the pixel values are reflectance. If the pixel values were not reflectance, the transformation from Digital Number (DN) to reflectance would have been applied; it is widely explained in several papers [20,21,22,23,24] and can be summarized in the following steps:

- Atmospheric Correction and cloud masking;
- Geometric resampling and geographic registration;
- BRDF (bidirectional reflectance distribution function) normalization;
- Band pass adjustment.

Behavior of the burned vegetation

Based on the analysis of the spectral signature of the pixel in the burned areas (pre and post-fire), it is possible to extract information using Red, Near Infrared and Shortwave infrared band.

In the case of healthy vegetation, the Red band shows a high contrast and at the same time provides a clear separation between vegetated areas and uncovered soils. In addition, this region is also extremely important for its sensitivity to chlorophyll concentration in vegetation. In the NIR region, the absorbance of vegetation is low whereas reflectance and transmittance are high.

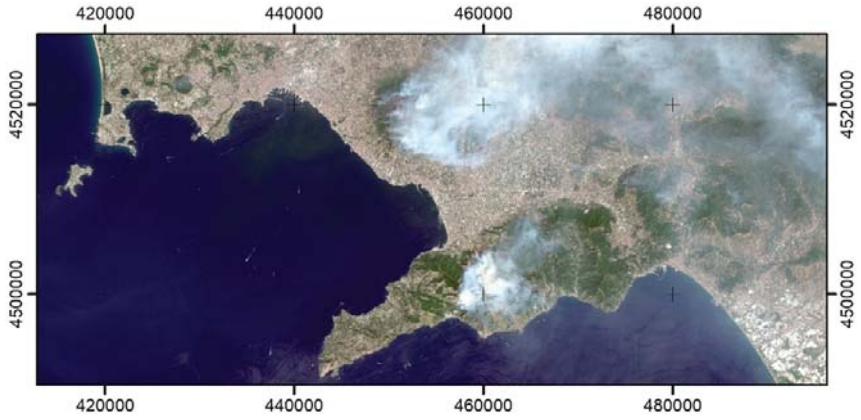

a)

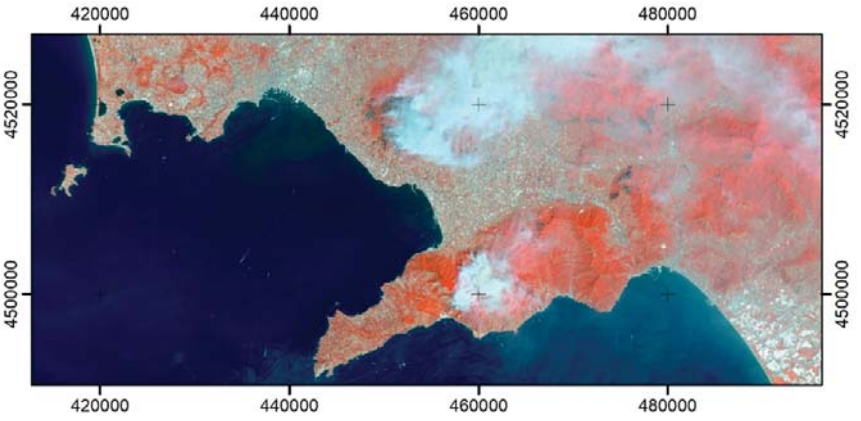

b)

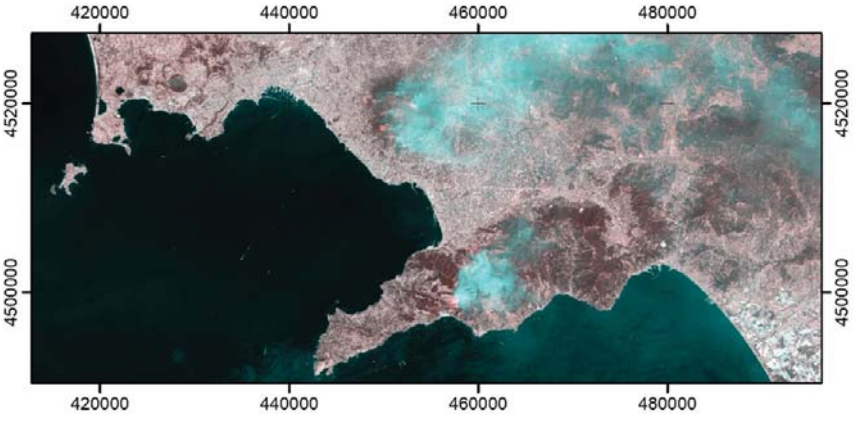

c)

Figure 1: Images of the study area taken by the Copernicus Sentinel-2B satellite recorded on 12 July 2017
a) Visible (Red-Green-Blue, composite bands);
b) Color Infrared (Red-Green-Near Infrared, composite bands);
c) False color (Red-Green-Short Wave Infrared composite bands)

In the SWIR region, the reflectance and transmittance of the vegetation are low and the absorbance is very high [25]. In the post-fire zone, the recently burned areas show a relatively low reflectivity in the near infrared, a very low reflectance in the red band and a high reflectance in the short wave infrared band.

The behavior of the burns and healthy vegetation region, regarding the reflectance values in the electromagnetic spectrum, can be sketched in the following graph (Figure 2). In addition, in the following graph are reported, varying the wavelength, the band number of Sentinel-2 used for the calculation of remote sensing indexes.

Use of the SWIR band in Sentinel-2 dataset

While in the case of images derived from Landsat 8 OLI, an American Earth observation satellite developed in collaboration between NASA and the United States Geological Survey (USGS) the *Red, Infrared and Short-wave-Infrared bands* have the same geometric resolution (30m), this does not occur in the case of Sentinel-2 images. Indeed, the SWIR band has a geometric resolution of 20m while the *NIR* and *Red* bands have one of 10m. Some authors used the pan-sharpening methods in order to increase the geometric resolution of the SWIR band. However, this method, widespread in order to increase the geometric resolution in visible range thanks to the acquisition of the pan-chromatic band, cannot be used in this way. Indeed, the panchromatic band covers only a visible part of the spectral wavelength range and does not cover the part beyond the *NIR* band. Also, it is not correct to use pan-sharpening method to increase the geometric resolution of *SWIR* band. In fact, in order to preserve the original physical value, the calculation of NBR was performed by sample ratio between the bands setting the spatial resolution of the output raster with the highest geometric resolution, i.e. that *Red* or *Infrared band* (10m).

Method

In order to identify the burned areas, a different procedure in relation to remote sensing index considered was adopted. In particular, for the identification of the burned areas by *NDVI*, the first step was the classification of the pre and post-fire images in three classes: soil, vegetation and water. The identification of the thresholds was carried out empirically using the criterion of *Maximum Likelihood* (ML). This task was carried out in ArcGIS software using the tool called "*Maximum Likelihood Classification*" which it is based on two principles: the cells in each class sample in the multidimensional space are normally distributed and Bayes' theorem of decision making. The result of the classification is shown in the Figure 3.

After the classification, the direct comparison technique was applied to the vegetation class according the Formula 5:

$$dNDVI_{Vegetation}\,\mathrm{map} = \mathrm{NDVI}_{Vegetation\,(pre-fire)}\mathrm{map} - \\ - \mathrm{NDVI}_{Vegetation\,(post-fire)}map \quad (5)$$

The resulting map of the change detection analysis on the vegetation class obtained by *NDVI* index, is shown in Figure 4 where the red pixels are potential burned areas.

As concerns the NBR index, once calculated the index on the pre and post-fire images, the difference map was calculated using the Formula 6:

$$\mathrm{dNBRmap} = \mathrm{NBR}_{pre-fire}\mathrm{map} - \mathrm{NBR}_{post-fire}map \quad (6)$$

This task was carried out by ArcGIS software using raster calculator tool. The difference map obtained by these indexes is shown in the Figure 5.

Once the difference dNBR map was generated, it was necessary to create a severity fire map. This means to identify a suitable threshold value in order to discern the burned areas. For example, for dNBR map, the USGS FireMon program [26], a National Burn Severity Mapping Project of the U.S. Geological Survey, indicates severity layer variable [27], as shown in the Table 1. The levels referred to the burned areas are divided in different classes.

Table 1: Ordinal severity levels range of dNBR, scaled by 10^3

dNBR	Burn Severity
< -251	High post-fire regrowth
-250 to -101	Low post-fire regrowth
-100 to 99	Unburned
100 to 269	Low-severity burn
270 to 439	Moderate-low severity burn
440 to 659	Moderate-high severity burn
> 660	High-severity burn

Because these indexes can vary in relation to the scene, the threshold value was obtained by iterative method on some test areas, starting from the values reported in the Table 3. The optimal value achieved for NBR index was 0.21. The threshold value was obtained using as training some burned areas derived by photo-interpretation on Sentinel-2 images.

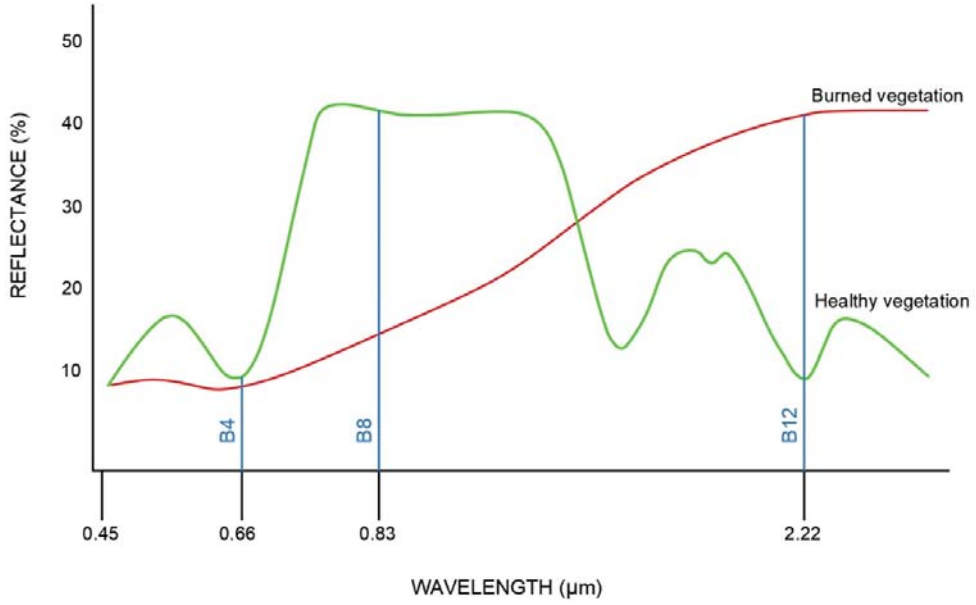

Figure 2: Reflectance values in electromagnetic spectrum

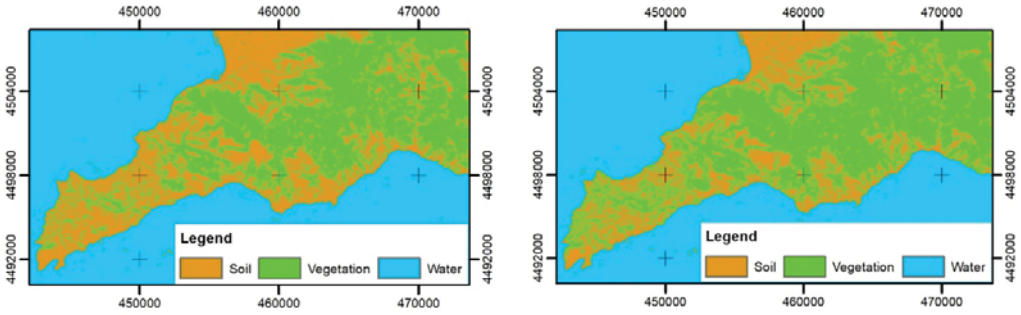

a) b)

Figure 3: Classification of Sentinel images in three classes
a) pre-fire classification map; b) post-fire classification map

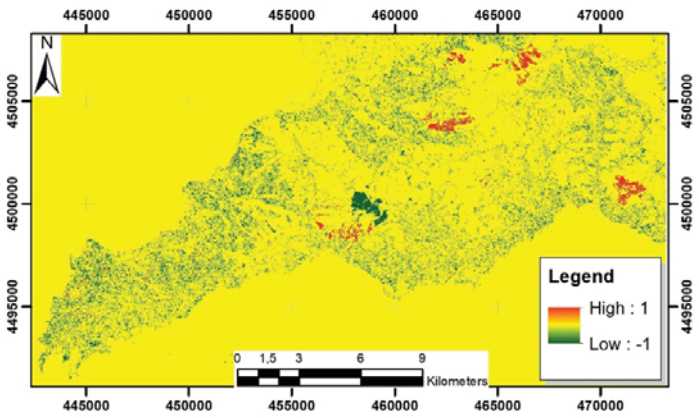

Figure 4: Map of difference using NDVI index

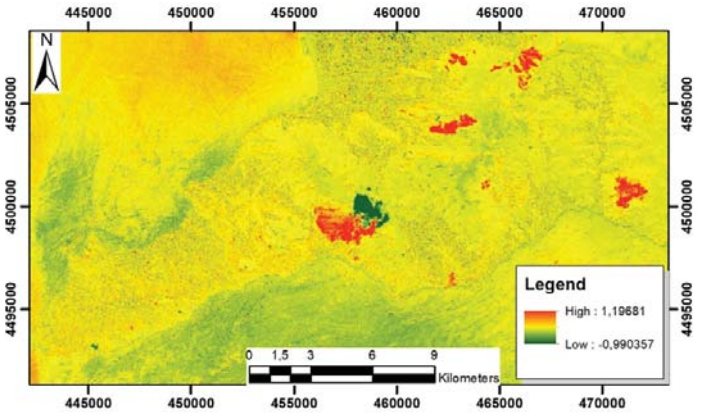

Figure 5: Map of difference using NBR index

Accuracy workflow

The verification of the thematic map accuracy produced by two indexes tested is usually expressed through the *error matrix* (also known as the *confusion matrix or contingency table*). The error matrix compare, on a class basis, the relationship between (known) reference data, and the corresponding results of the classified image. In this case study, the true data has been carried out by photo-interpretation using Sentniel-2 image and images derived from very high resolution optical satellites.

The further data available that confirming the exact burned areas was provided from the register (database) of the fires drafted by local public administration.

In order to build the confusion matrix, through the use of a tool developed in ArcMap environment called "*Zonal Statistic as Table*", it was possible to extract the statistical parameters. Therefore, the workflow implemented in *ArcGIS* software needs to obtain the accuracy value of the thematic map produced by each remote sensing used, is shown below (Figure 6). Lastly, once build the confusion matrix, using *Matlab* software, the several parameters accuracy processing were performed.

In order to analyze the quality of the remote sensing indexes tested, several accuracy methods were used [28,29]: *User's Accuracy* (UA), *Producer's Accuracy* (PA), *Overall Accuracy* (OA) and *Kappa coefficient* ($\hat{k}$). The first two indexes provide an estimate of the thematic accuracy of each class considered, while the last two provide a global assessment of the degree of accuracy achieved by the classification [30]. The *User's Accuracy* of the class i (UAi), can be defined as the ratio between the number of pixels correctly classified in the burn class and the total number of pixels assigned to that class while the *Producer's Accuracy* of the class j (PAj), can be defined as the ratio between the total of the correct pixels of the class j and the total number of pixels of that class present in the reference (column total). The *Overall Accuracy* of the classified image compares how each of the pixels is classified in or not buns area obtained from their corresponding ground truth data and it can be defined as the ratio between the total number of correctly classified pixels (the elements present on the diagonal) and total number of pixels in the error matrix. The last method used for experimentation is the *Kappa coefficient* (also known as *Kappa hat or K-hat coefficient*), compares the number of pixels in each cell in the error matrix with the possibility to distribute pixels as a random variable and can be calculated by Formula 7 [31]:

$$\hat{k} = \frac{N \sum_{i=1}^{m} D_{ij} - \sum_{j=1}^{m} R_i \cdot C_j}{N^2 - \sum_{j=1}^{m} R_i \cdot C_j} \qquad 7)$$

where

N total number of pixels;

m number of classes;

D_{ij} total diagonal elements of an error matrix;

R_i total number of pixels in row i;

C_j total number of pixels in column j.

RESULTS AND DISCUSSIONS

In the area under investigation were recognized 35 burned areas distributed over a region of over 700 hectares. The accuracy parameters achieved by NBR index are shown in the following Table 2.

Table 2: Accuracy achieved for NBR index, excluding the surfaces covered by water from the observed scene

	UA	*PA*	*OA*	$\hat{k}$
burns	84.5%	87.8%		
NO	99.7%	99.6%	99.3%	85.7%

The accuracy parameters achieved by NDVI index in the study area, are shown in the following table (Table 3).

Table 3: Accuracy achieved for NDVI index

	UA	*PA*	*OA*	$\hat{k}$
burns	39.0%	37.9%		
NO	98.2%	98.3%	96.7%	36.7%

From the observation of the Table 2, it is possible to note the high performances achievable by *dNBR* in order to recognize the burned areas. Instead, from the analysis of the Table 3, it was highlighted the poor performance of the *NDVI* index in the recognition of burned areas. Indeed, in a large and defined area, due of a type of vegetation that had a low *NDVI* index both pre and post-fire, the use of the *dNDVI* was not able to recognize this area as burned. Therefore, the use of the *NDVI* index in the identification of the burns area should be used carefully. In addition, the difference *NDVI* map show only if a pixel belong the vegetal layer is change or not, but without specifying if such the change was caused by a fire or other factors.

Therefore, if the works present at moment in the literature showed a little difference in terms of accuracy in the recognition of the burned areas between the *NBR* and *NDVI* index [09, 10], in this paper it was showed that strong differences between these indexes can result in particular cases. In other word, it was established that the use of the index *NDVI* in presence of some type of vegetation as well as mixture vegetation/soil, can be unsuitable for the recognition of the burned areas.

Journal of Applied Engineering Science Vol. 16, No. 2, 2018
ISSN 1451-4117

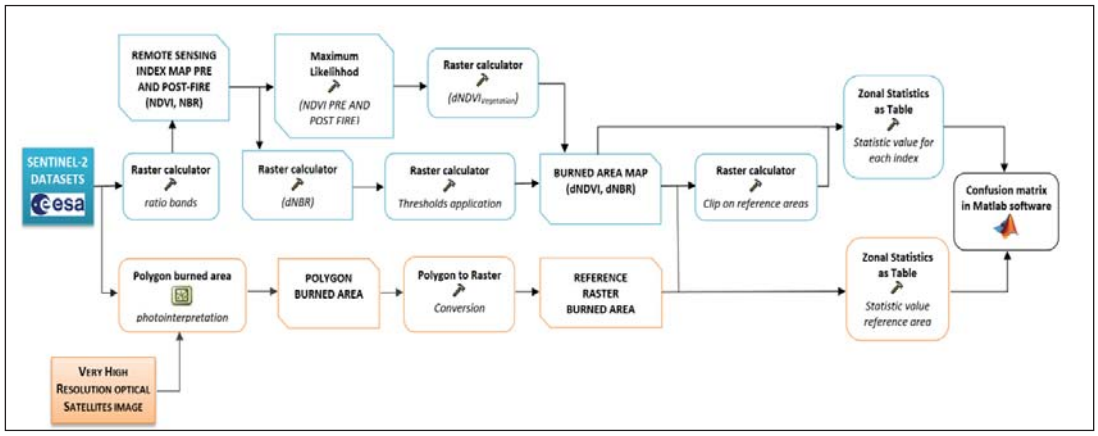

Figure 6: Workflow developed in order to build the confusion matrix

CONCLUSIONS

Using change detection analysis on Sentinel-2A images and using *NBR* index, it was possible to identify the burned area in the Sorrento Peninsula and, as consequence, to build with elevated accuracy the map of this region.

Regarding the continuity of acquisition of the Sentinel-2 sensor between two dates of interest, it was possible to get images of the study area pre and post-fire and, of consequence, to document, analyze and investigate a specific phenomenon. Indeed, the Sentinel constellation satellites allows covering all surfaces of the Earth between the latitudes 84°S and 84°N every five days. Therefore, the ability to continuously acquire represents a valid and excellent tool for monitoring burned areas through satellite images.

Lastly, considering the high geometric resolution achieved by Sentinel-2 dataset, it was possible to identify even the small burned areas. Indeed, in this case study, it was possible to obtain even the recognition of areas with an extension of 1000m^2. This characteristic becomes very important especially in urban and semi-urban landscape, both in order to impose urban planning constraints and to establish/plan sustainable interventions on burned areas.

ACKNOWLEDGMENT

This research was part of the "*Change detection techniques applied to satellite images for the identification of expansions of the built territory*", a research project supported by University of Naples "*Parthenope*".

In addition, we want to thank the anonymous reviewers for constructive comments concerning our manuscript.

REFERENCES

1. Bovio, G., Marchetti, M., Tonarelli, L., Salis, M., Vacchiano, G., Lovreglio, R., Elia, M., Fiorucci P., Ascoli, D. (2017).Gli incendi boschivi stanno cambiando: cambiamo le strategie per governarli. Forest@-Journal of Silviculture and Forest Ecology, vol.14 no.5, 202.
2. Vilar, L., Camia, A., & San-Miguel-Ayanz, J. A comparison of remote sensing products and forest fire statistics for improving fire information in Mediterranean Europe. (2015). European Journal of Remote Sensing, vol. 48 no.1, pp. 345-364.
3. Chowdhury, E. H., Hassan, Q. K. (2015) Operational perspective of remote sensing-based forest fire danger forecasting systems. ISPRS Journal of Photogrammetry and Remote Sensing, vol. 104, 224-236.
4. Singh, A. Digital Change Detection Techniques Using Remotely Sensed Data (1989). International Journal of Remote Sensing, vol.10 no.6, pp. 989-1003.
5. Tucker, CJ. (1979). Red and photographic infrared linear combinations for monitoring vegetation. Remote sensing of environment, vol.8, 127–150.
6. Ding, Y., Zhao, K., Zheng, X., Jiang, T. (2014). Temporal dynamics of spatial heterogeneity over cropland quantified by time-series NDVI, near infrared and red reflectance of Landsat 8 OLI imagery. International Journal of Applied Earth Observation and Geoinformation, vol.30, 139-145.
7. Ireland, G., Petropoulos, G. P. (2015). Exploring the relationships between post-fire vegetation regeneration dynamics, topography and burn severity: A case study from the Montane Cordillera Ecozones of Western Canada. Applied Geography. Vol. 56, pp.232-248.
8. Pepe M. (2017). Use of Digital Aerial Photogrammetry Sensors for Land Cover Classification, International Journal of Applied Engineering Research, vol.12 no.24, pp.15610-15620.

9. Fernández, A., Illera, P., Casanova, J. L. (1997). Automatic mapping of surfaces affected by forest fires in Spain using AVHRR NDVI composite image data. Remote sensing of environment, vol.60 no.2, 153-162.
10. Chuvieco, E., Martin, M. P., Palacios, A. (2003). Assessment of different spectral indexes in the red-near-infrared spectral domain for burned land discrimination. International Journal of Remote Sensing, vol.23 no.23, 5103-5110.
11. Warner, T. A., Skowronski, N. S., Gallagher, M. R. (2017). High spatial resolution burn severity mapping of the New Jersey Pine Barrens with WorldView-3 near-infrared and shortwave infrared imagery. International Journal of Remote Sensing. vol.38 no.2, 598-616.
12. Key, C. H., Benson, N. (1999). The Normalized Burn Ratio (NBR): A Landsat TM radiometric index of burn severity incorporating multitemporal differencing.
13. Miller, J. D., Yool, S. R. (2002). Mapping forest post-fire canopy consumption in several overstory types using multi-temporal Landsat TM and ETM data. Remote Sensing of Environment, vol.82, no.3, 481−496.
14. Zhihua, L., Jian Y., Francis Dwomoh. (2016). Mapping recent burned patches in Siberian larch forest using Landsat and MODIS data, European Journal of Remote Sensing, vol.49, 861-887.
15. Miller, J. D., Thode, A. E. (2007). Quantifying burn severity in a heterogeneous landscape with a relative version of the delta Normalized Burn Ratio (dNBR). Remote Sensing of Environment, vol.109 no.1, 66-80.
16. Fang, L., Yang, J. (2014). Atmospheric effects on the performance and threshold extrapolation of multi-temporal Landsat derived dNBR for burn severity assessment. International Journal of Applied Earth Observation and Geoinformation, vol.33, 10-20.
17. Government agency “Monti Lattari regional Park”. (2018). (Last accessed: 25/01/2018). Available on line: http://www6.asmenet.it/enteparcodeimontilattari/index.php?action=index&p=328
18. Drusch, M., Bello, U.D., Carlier, S., Colin, O., Fernandez, V., Gascon, F., Hoersch, B., Isola, C., Laberinti, P., Martimort, P. (2012). Sentinel-2: ESA's optical high-resolution mission for GMES operational services. Remote Sens. Environ. vol.120, 25–36.
19. Immitzer, M., Vuolo, F., Atzberger, C. (2016). First experience with Sentinel-2 data for crop and tree species classifications in central Europe. Remote Sensing, vol.8 no.3, 166.
20. Chander, G., Markham, B. L., Helder, D. L. (2009). Summary of current radiometric calibration coefficients for Landsat MSS, TM, ETM+, and EO-1 ALI sensors. Remote sensing of environment, vol. 113, no.5, 893-903.
21. Blackett, M. (2014). Early analysis of Landsat-8 thermal infrared sensor imagery of volcanic activity. Remote sensing, vol.6, no.3, 2282-2295.
22. Baillarin, S., Meygret, A., Dechoz, C., Petrucci, B., Lacherade, S., Tremas, T., Isola, C., Martimort, P., Spoto, F. (2012). Sentinel-2 level 1 products and image processing performances. In Proceedings of 2012 IEEE International Geoscience and Remote Sensing Symposium (IGARSS 2012), Munich, Germany, 22–27 July 2012, 7003–7006.
23. Baillarin, S. J., Meygret, A., Dechoz, C., Petrucci, B., Lacherade, S., Tremas, T., ... , Spoto, F. (2012). Sentinel-2 level 1 products and image processing performances. In Geoscience and Remote Sensing Symposium (IGARSS), IEEE International, 7003-7006.
24. Parente, C., Pepe, M. (2018). Bathymetry from worldview-3 satellite data using radiometric band ratio, Acta Polytechnica, vol. 58, no.2, 109-117.
25. Roy, D. P., Zhang, H. K., Ju, J., Gomez-Dans, J. L., Lewis, P. E., Schaaf, C. B., ... , Kovalskyy, V. (2016). A general method to normalize Landsat reflectance data to nadir BRDF adjusted reflectance. Remote Sensing of Environment, vol. 176, 255-271.
26. Park, H., Choi, J., Park, N., Choi, S. (2017). Sharpening the VNIR and SWIR Bands of Sentinel-2A Imagery through Modified Selected and Synthesized Band Schemes. Remote Sensing, vol.9, no 10,1080.
27. Lutes, DC, Keane, RE, Caratti, JF, Key, CH, Benson NC, Sutherland, S, Gangi, LJ. (2006). FIREMON: The fire effects monitoring and inventory system. USDA Forest Service, Rocky Mountain Research Station General Technical Report RMRS-GTR-164-CD.
28. Brivio, P., Lechi, G., Zilioli, E. (2006). Principi e metodi di telerilevamento. CittaStudi. pp. 413-415.
29. Liu, C., Frazier, P., Kumar, L. (2007). Comparative assessment of the measures of thematic classification accuracy. Remote sensing of environment, vol.107 no.4, 606-616.
30. Safford, H. D., Miller, J., Schmidt, D., Roath, B., Parsons, A. (2008). BAER soil burn severity maps do not measure fire effects to vegetation: a comment on Odion and Hanson (2006). Ecosystems. vol.11, no.1, 1-11.
31. Bogoliubova, A., Tymków, P. (2014). Accuracy assessment of automatic image processing for land cover classification of St. Petersburg protected area. Acta Scientiarum Polonorum. Geodesia et Descriptio Terrarum, vol. 13, 5-22.

Paper submitted: 23.04.2018.
Paper accepted: 29.05.2018.